

The Structure of the $[\text{Zn}_{\text{In}}\text{-V}_{\text{P}}]$ Defect Complex in Zn Doped InP.

C.W.M. Castleton and S.Mirbt
Theory of Condensed Matter,
Department of Physics, Uppsala University,
*Box 530, 751 21 Uppsala, Sweden.**
 (Dated: July 4, 2021)

We study the structure, the formation and binding energies and the transfer levels of the zinc-phosphorus vacancy complex $[\text{Zn}_{\text{In}}\text{-V}_{\text{P}}]$ in Zn doped p-type InP, as a function of the charge, using plane wave ab initio DFT-LDA calculations in a 64 atom supercell. We find a binding energy of 0.39 eV for the complex, which is neutral in p-type material, the 0/-1 transfer level lying 0.50 eV above the valence band edge, all in agreement with recent positron annihilation experiments. This indicates that, whilst the formation of phosphorus vacancies (V_{P}^{+1}) may be involved in carrier compensation in heavily Zn doped material, the formation of Zn-vacancy complexes is not.

Regarding the structure: for charge states $Q = +6 \rightarrow -4$ the Zn atom is in an sp^2 bonded DX position and electrons added/removed go to/come from the remaining dangling bonds on the triangle of In atoms. This reduces the effective vacancy volume monotonically as electrons are added to the complex, also in agreement with experiment. The reduction occurs through a combination of increased In-In bonding and increased Zn-In electrostatic attraction. In addition, for certain charge states we find complex Jahn-Teller behaviour in which up to three different structures, (with the In triangle dimerised, antidimerised or symmetric) are stable and are close to degenerate. We are able to predict and successfully explain the structural behaviour of this complex using a simple tight binding model.

PACS numbers: 71.55.Eq 61.72.Bb 71.70.Ej 71.15.Dx

I. INTRODUCTION

Zn doped p-type InP is one of the most common materials in use within optoelectronics. The Zn sits substitutionally within the In sublattice (Zn_{In}) where it has a shallow acceptor level. A well known limitation in the use of Zn as a p-dopant in InP is the saturation of the hole concentration in the mid 10^{18} cm^{-3} range. Above this further increases in Zn concentration do not translate into increases in hole concentration. There are several suspected causes¹ for this, in particular: a) increases in the concentration of interstitial zinc (Zn_{i}), b) phase separation and c) the formation of other compensating defects, especially phosphorus vacancies¹ (V_{P}) and complexes of zinc with V_{P} . In this paper we will examine the properties of Zn- V_{P} complexes, using ab initio methods.

The formation of one such Zn- V_{P} complex has recently been studied^{2,3} by Slotte et al. in Zn doped Czochralski grown samples which have been post-growth annealed in the temperature range 300-600 K. Using positron annihilation they find that the complex has at least two forms. The most stable at room temperature² has an effective vacancy volume larger⁴ than that of a free V_{P} . A binding energy on the order of $0.1 \rightarrow 0.4$ eV is anticipated³ (prior to detailed measurements). When the measurement temperature is raised they find that the complex undergoes a transition to a form with a smaller vacancy volume, similar to that of the free vacancy. It has been suggested that the more stable form is neutral² and has a DX structure³ which becomes non-DX when excited to the -1 charge state. They find² the 0/-1 transfer level 0.2 ± 0.1 eV above the valence band edge.

A number of theoretical studies of the free phosphorus vacancy have been performed^{5,6,7} using Density Functional Theory (DFT). The free vacancy has been shown^{6,7} to be a strong Jahn-Teller defect, indeed, to be a “negative U” centre in which the neutral charge state V_{P}^0 is thermodynamically unstable relative to the +1 and -1 states. Hence a direct change $\text{V}_{\text{P}}^{-1} \rightarrow \text{V}_{\text{P}}^{+1}$ occurs as a function of increasing electron chemical potential (Fermi level). This is due to strong lattice relaxation in the -1 charge state. The vacancy is surrounded by a tetrahedron of four In atoms, each with a (partially filled) inwardly pointing dangling bond. In the -1 charge state a pair of dimers is formed: two opposing sides of the tetrahedron are reduced in length relative to the remaining four. The energy gained by this overcomes the Coulomb repulsion between the additional electrons, allowing two electrons to be transferred onto the vacancy simultaneously.

In this paper we present what is, to our knowledge, the first ab initio¹⁹ ab initio theoretical study of the $[\text{Zn}_{\text{In}}\text{-V}_{\text{P}}]$ complex, which we propose to be that observed in the positron annihilation experiments. We will first describe the method in section II. We will then report detailed results for the geometry and vacancy volume of the complex, both for the ground state structures and for various metastable structures in section III, followed by a description of how these vary with changes in the charge state of the complex in section IV. In section V we will also propose a simple tight binding model which is able to predict almost all of the structural properties which we find. Finally, in section VI we will conclude, relating our results to those from position annihilation and the issue of Zn compensation.

TABLE I: Comparison of the k-point convergence of the electronic and structural contributions to the formation energy, E_d . Convergence of the electronic contributions is given by the change, $\Delta^{UR}(\text{N-M})$, in the unrelaxed formation energy when increasing the k-point grid from NxNxN to and MxMxM. Convergence of the structural contributions is given by $\Delta^R(\text{N-M})$, the equivalent change in relaxation energy $\epsilon_R(\text{N})$. See main text for full definitions.

Defect	$\Delta^{UR}(2-4)$	$\Delta^{UR}(6-4)$	$\Delta^R(2-4)$
$\text{V}_{\text{In}}^{-4}$	0.0082		-0.0190
V_{In}^0	-0.0483	0.0093	0.0368
In_i^0	0.0252	0.0052	
In_i^{+1}	-0.0539		-0.0037
In_i^{+3}	0.0206	0.0058	
In_i^{+4}	-0.1038		0.0061
$\text{P}_{\text{In}}^{+1}$	-0.0360		0.0246
$\text{P}_{\text{In}}^{+2}$	0.0314		0.0259
V_{P}^{-2}	-0.0607	-0.0123	
V_{P}^{+2}	0.0840	0.0012	
$\text{Zn}_{\text{In}}^{+1}$	0.0375		0.0007
Zn_{In}^0	0.0807	-0.0011	-0.0025
$\text{Zn}_{\text{In}}^{-1}$	-0.0004	0.0000	-0.0005
ZnP^{+2}	-0.0266		0.0095
Zn_i^{+2}	0.0117	0.0001	0.0040
Si_{In}^0	0.0091		0.0091
$\text{Si}_{\text{In}}^{+1}$	0.0048		-0.0038
$\text{Si}_{\text{In}}^{+2}$	0.0891		0.0046
$\text{Si}_{\text{P}}^{-2}$	0.0296		-0.0006
$\text{Si}_{\text{P}}^{-1}$	0.0031		0.0008
Si_{P}^0	0.0734		-0.0027
$\text{Si}_{\text{P}}^{+1}$	0.0279		0.0004
$[\text{Zn}_i\text{-V}_{\text{P}}]^{+3}$	0.0272		0.0151
$[\text{Zn}_{\text{In}}\text{-V}_{\text{P}}]^{-1}$	-0.0750		0.0046
$[\text{Zn}_{\text{In}}\text{-V}_{\text{P}}]^0$	0.0057		-0.0029
$[\text{Zn}_{\text{In}}\text{-V}_{\text{P}}]^{+1}$	-0.0598		0.0184

II. CALCULATIONAL DETAILS.

We use planewave *ab initio* DFT⁸ within the Local Density Approximation (LDA) together with ultrasoft pseudopotentials^{9,10}. Calculations are performed using the VASP code¹¹. Before doing calculations involving defects we first optimise the lattice parameter subject to LDA. We find a value of 5.827 Å, compared to 5.869 Å experimentally, giving us a band gap of 0.667 eV, compared to 1.344 eV in experiment.

For defect calculations we use a 64 atom simple cubic supercell and allow all atoms not located on the surface of the cell to relax. This restriction is included to truncate the (spurious) elastic interactions between adjacent supercells. No restrictions are placed upon the symmetry of the relaxations. When calculating total energies of supercells containing charged defects we also include a uniform neutralising background charge. The key quantity is the formation energy of the defect, E_d , defined¹²

as

$$E_d = E^T(\text{defect}^Q) - E^T(\text{bulk}) + \sum_i \mu_i n_i + Q(e_v + e_f) \quad (1)$$

where $E^T(\text{defect}^Q)$ and $E^T(\text{bulk})$ are the total energy of the InP supercell with and without the charge Q defect. Both are calculated with the same values of planewave cutoff, k-point grid, etc, in order to make use of cancellation of errors. The defect is formed by adding(removing) n_i atoms, each with chemical potential μ_i , and by adding $(-Q)$ electrons, whose chemical potential e_f is measured from the valence band edge e_v . We then adjust the various calculational parameters to converge E_d . We find that it is sufficient to use pseudopotentials in which Zn d-electrons are treated as valence electrons but In d-electrons are left in the core. We find that a planewave cutoff energy of 200 eV is enough to converge E_d to $O(0.01 \text{ eV})$. Real space projection operators are used, with the cutoff again chosen to give errors below $O(0.01 \text{ eV})$.

The k-point convergence is more interesting, since we find different convergence behaviour for the electronic and structural contributions to the formation energy $E_d(\text{K})$, where we use a KxKxK Monkhorst-Pack¹³ k-point grid. The error in the electronic contribution to $E_d(\text{K})$ is very close to the error in the unrelaxed formation energy, $E_d^{UR}(\text{K})$, which we can estimate as

$$\Delta^{UR}(\text{N-M}) = E_d^{UR}(\text{N}) - E_d^{UR}(\text{M}) \quad (2)$$

(We shall use $\{\text{N,M}\} = \{2,4\}$ and $\{4,6\}$ to estimate the errors in $E_d^{UR}(2)$ and $E_d^{UR}(4)$ respectively.) We cannot, of course, calculate the structural contribution directly, so we first define the relaxation energy

$$\epsilon_R(\text{K}) = E_d^R(\text{K}) - E_d^{UR}(\text{K}) \quad (3)$$

where $E_d^R(\text{K})$ is the relaxed formation energy. We then estimate the convergence of $\epsilon_R(\text{K})$ using

$$\Delta^R(\text{N-M}) = \epsilon_R(\text{N}) - \epsilon_R(\text{M}) \quad (4)$$

In table I we list values of $\Delta^{UR}(2-4)$, $\Delta^{UR}(4-6)$ and $\Delta^R(2-4)$ for a range of charge states of various different defects in InP. We find that when atomic relaxations are ignored, a 2x2x2 k-point grid produces errors below $O(0.01 \text{ eV})$, provided $Q = 0$. (Column $\Delta^{UR}(2-4)$ of table I.) When $Q \neq 0$, however, we find that the error introduced by truncating at 2x2x2 increases with $|Q|$. Instead, a 4x4x4 grid is required: column $\Delta^{UR}(4-6)$ indicates that this is sufficiently converged. On the other hand, the relaxation energy $\epsilon_R(\text{K})$ converges faster, see column $\Delta^R(2-4)$ in the table. Indeed, $\epsilon_R(\text{K})$ is converged for a 2x2x2 Monkhorst-Pack grid, for any value of Q . In other words the structural contribution to E_d appears to converge faster with k-point grid than the electronic contributions. This is largely due to a double cancellation of errors when we calculate ϵ_R from values of E_d which already contain a cancellation of errors. It means that,

TABLE II: Transfer levels of $[\text{Zn}_{\text{In}}\text{-V}_{\text{P}}]$, in the 64 atom cell, relative to the valence band edge.

Level	Energy
+6/+5	-0.51 eV
+5/+4	-0.51 eV
+4/+3	-0.47 eV
+3/+2	-0.44 eV
+2/+1	-0.37 eV
+1/0	-0.32 eV
0/-1	0.50 eV
-1/-2	0.70 eV
-2/-3	0.95 eV
-3/-4	1.05 eV
-4/-5	1.19 eV
-5/-6	1.18 eV

TABLE III: Geometry of the most stable form of $[\text{Zn}_{\text{In}}\text{-V}_{\text{P}}]^Q$ as a function of Q . Distances in Å, volumes in Å³. Most structures (Str.) found are symmetric (SY) (all In-In distances equal, all Zn-In distances equal.) Where the In-In (and likewise Zn-In) distances differ it is found that two remain equal (In-In(2)) and one is different (In-In(1)) by amount $\Delta(\text{In})$. ($\text{In} - \text{In}(1) < (\text{In} - \text{In}(2))$) corresponds to the formation of a dimer (DM) and ($\text{In} - \text{In}(1) > (\text{In} - \text{In}(2))$) to an antidimer (AD).

Q	Zn-P	Zn-In		In-In		Volume	Str.	$\Delta(\text{In})$
		(1)	(2)	(1)	(2)			
+6	2.29	4.97		4.95		14.36	SY	
+5	2.29	4.97		4.96		14.42	SY	
+4	2.29	4.98		4.97		14.49	SY	
+3	2.29	4.97		4.99		14.53	SY	
+2	2.29	4.99		4.97		14.57	SY	
+1	2.30	4.69		4.36		10.86	SY	
+0	2.30	4.41		3.69		7.58	SY	
-1	2.30	4.23	4.31	3.64	3.37	6.52	AD	7.9%
-2	2.31	4.13	4.20	3.52	3.19	5.81	AD	10.3%
-3	2.32	3.95	4.10	2.99	3.28	5.23	DM	8.9%
-4	2.32	3.96		3.08		4.85	SY	
-5	2.43	3.21		3.04		3.59	SY	
-6	2.51	2.99		2.95		3.09	SY	

although we should use a 4x4x4 grid to obtain an accurate value for E_d^R , we can save much calculation time by estimating $E_d^R(4)$ as

$$\begin{aligned} E_d^R(4) &\approx E_d^{UR}(4) + \epsilon_R(2) \\ &= E_d^{UR}(4) + E_d^R(2) - E_d^{UR}(2) \end{aligned} \quad (5)$$

The resulting values of $E_d^R(4)$ are converged to at least 0.02-0.04 eV, and usually to an order of magnitude or so better. Hence we do most relaxations with a 2x2x2 k-point grid, only checking key ones at 4x4x4. Charge and Electron Localisation Function¹⁴ (ELF) plots are, on the other hand, calculated using a 4x4x4 k-point grid at the 2x2x2 related structures.

TABLE IV: Geometry of structural excitations of $[\text{Zn}_{\text{In}}\text{-V}_{\text{P}}]^Q$ as a function of Q . Energies are given relative to the energy of the most stable structures, as listed in table III. See table III also for meaning of other columns and notation.

Q	Energy [eV]	Zn-P	Zn-In		In-In		Volume	Str.	$\Delta(\text{In})$
			(1)	(2)	(1)	(2)			
+4	1.00	2.30	4.44		3.74		7.85	SY	
+3	0.97	2.30	4.44		3.76		7.91	SY	
+2	0.93	2.30	4.44		3.72		7.76	SY	
+1	0.12	2.30	4.42		3.71		7.67	SY	
-1	0.011	2.30	4.29	4.27	3.41	3.50	6.57	DM	2.7%
-1	0.012	2.30	4.28		3.47		6.58	SY	
-2	0.03	2.31	4.18	4.17	3.22	3.35	5.85	DM	3.7%
-3	0.02	2.31	4.05	4.10	3.41	3.06	5.26	AD	11.6%
-3	0.05	2.31	4.08		3.18		5.31	SY	
-5	0.02	2.34	3.67		3.05		4.32	SY	
-6	0.19	2.34	3.63		3.05		4.26	SY	

III. THE NEUTRAL $[\text{Zn}_{\text{In}}\text{-V}_{\text{P}}]$ COMPLEX.

A. Formation and Binding Energies.

In order to calculate absolute values for the formation and binding energies we need to know the chemical potentials μ_{In} , μ_{P} and μ_{InP} . Fully converged calculations for In, P (black phosphorus) and InP (the latter in its basic 2 atom FCC cell) give the bulk values²⁰ -3.270 eV, -6.028 eV and -9.728 eV respectively. For pure InP we have, at thermodynamic equilibrium, $\mu_{\text{InP}} = \mu_{\text{In}} + \mu_{\text{P}}$. In In rich material we then have $\mu_{\text{In}} = -3.270$ eV leading to $\mu_{\text{P}} = -6.459$ eV, whilst in P rich material $\mu_{\text{P}} = -6.028$ eV and hence $\mu_{\text{In}} = -3.700$ eV. We now use the values $\mu_{\text{In}} = -3.485$ eV and $\mu_{\text{P}} = -6.243$ eV, corresponding to exactly stoichiometric conditions. Properly, doping with Zn should alter these μ values, but even a Zn concentration of $5.10^{18} \text{ cm}^{-3}$ only corresponds to replacing 1 In in 2000 with Zn. We thus ignore the effect, and use the fully converged bulk value -1.891 eV for μ_{Zn} .

Since we are primarily interested in strongly p-type material, we assume that the electron chemical potential lies at the valence band edge, meaning that $e_f = 0$. Using fully relaxed calculations in the 64 atom simple cubic cell, we find that the most stable charge states of the Zn_{In} and V_{P} are -1 and +1 respectively, whilst for $[\text{Zn}_{\text{In}}\text{-V}_{\text{P}}]$ it is 0. The formation energies are $E_d(\text{Zn}_{\text{In}}^{-1}) = 0.32$ eV, $E_d(\text{V}_{\text{P}}^{+1}) = 1.96$ eV and $E_d([\text{Zn}_{\text{In}}\text{-V}_{\text{P}}]^0) = 1.89$ eV. For V_{P} we find a free vacancy volume of 6.5 Å^3 , where we calculate only the volume of the tetrahedron formed by the four In surrounding the vacancy. V_{P}^{+1} is invisible to positrons, so we will also report here the volume of V_{P}^{-1} , which is 4.6 Å^3 . More detailed results about V_{P} and Zn_{In} will appear elsewhere.¹⁵

We can evaluate the binding energy, E_b , of the complex

as

$$E_b([\text{Zn}_{\text{In}}\text{-V}_{\text{P}}]^0) = E_d(\text{Zn}_{\text{In}}^{-1}) + E_d(\text{V}_{\text{P}}^{+1}) - E_d([\text{Zn}_{\text{In}}\text{-V}_{\text{P}}]^0) \quad (6)$$

This gives us a value of 0.39 eV, which agrees with the 0.1 \rightarrow 0.4 eV estimate from the positron annihilation experiments³.

B. Structure.

In figure 1 we show the relaxed structure of the $[\text{Zn}_{\text{In}}\text{-V}_{\text{P}}]$ complex in the $Q = 0$ charge state. The Zn_{In} is bonded to three P atoms only and has relaxed back into a DX-like position in the same plane as those P atoms. The resulting Zn-P distances are 2.31 Å, which is almost identical to the 2.34 Å value we find for the shorter Zn-P distances in a similar DFT-LDA calculation for Zn_3P_2 and various other Zn-P binary compounds.¹⁶ The three In atoms on the other side of the V_{P} have moved together slightly, giving three equal In-In distances of 3.69 Å, compared to an ideal LDA bulk next nearest neighbour distance of 4.12 Å. The Zn-In distance is rather longer than the bulk value, however, at 4.41 Å. This gives a volume for the vacancy of 7.58 Å³, where we calculate simply the volume of the tetrahedron formed by the three In and the Zn. In the remaining figures most of the atoms in the cell are omitted for clarity, and lines are drawn around the edges of the tetrahedron to guide the eye. In the case of Zn-In lines they do *not* represent bonds. This can be seen clearly by examining the ELF¹⁴ plots in figure 2. There is no ELF density at all between the Zn and the In triangle, indicating that there is no bonding between them. Instead, the Zn has three sp^2 hybrid orbitals bonded to the surrounding P, these bonds being filled. There is no density related to the Zn at all along the line perpendicular to the Zn-P plane (the (111) axis). This indicates that the single Zn $2p^z$ orbital left over from the formation of the sp^2 hybrids is empty.

IV. THE STRUCTURE OF $[\text{Zn}_{\text{In}}\text{-V}_{\text{P}}]$ AS A FUNCTION OF CHARGE STATE.

A. Bond lengths and vacancy volumes.

In table II we give the positions of a number of transfer levels of the complex. The structures of all of the states we have examined (+6 \rightarrow -6) are very similar, as listed in table III. For all $Q > -5$ the Zn lies in the DX-like position. The three In atoms remain unbonded to Zn, but both the In-In distances and the Zn-In distances shorten with increasing negative charge. This reduces the vacancy volume for each additional electron. This holds until $Q = -5$, when the Zn $2p^z$ orbital starts to be filled, leading at $Q = -6$ to a non-DX position for the Zn atom, with the Zn-In distance only 1.6% longer than the In-In. The transfer level into this state lies

1.18 eV above the valence band edge. With the LDA band gap being only 0.67 eV this places the level about 0.51 eV above the conduction band edge. This orbital also displays a negative U effect: the $Q = -5$ structure - which lies half way between DX and non-DX forms - is thermodynamically unstable, so the transfer level -5/-6 lies just below the -4/-5 level. Hence we anticipate instead a -4/-6 level about 0.5 eV above the conduction band edge.

In addition to this, for $Q = -1 \rightarrow -3$, Jahn-Teller effects are apparent, in which one In-In distance is shortened (dimerised) or lengthened (antidimerised) relative to the other two. These remaining In-In distances always remain equal to at least 0.001 Å.

In table IV we show the various metastable structures (structural excitations) which we find. (An extensive search suggests that there are no other metastable structures besides these.²¹ The fact that the Zn $2p^z$ level lies well inside the conduction band is further underlined by the metastable structures seen for $Q = -5$ and $Q = -6$. For both of these we find a DX-like metastable structure very similar to the ground state structure of the $Q = -4$ state. This indicates that one or two electrons (respectively) have been transferred from the complex into the conduction band, leaving the complex with an empty Zn $2p^z$ and additional charge elsewhere in the supercell. The energy splitting between these DX and non-DX forms is therefore expected to change significantly (indeed, to switch over) in larger supercells where less defect level dispersion is seen. A similar effect is seen in the $Q = +1 \rightarrow +4$ charge states, where a metastable structure is found which closely resembles the $Q = 0$ structure. Since the hole levels corresponding to these charge states lie below the valence band edge, these structural excitations amount to exciting holes off the complex, leaving it in the $Q = 0$ charge state, with additional charge elsewhere. (An equivalent structural excitation for $Q = +5$ or +6 has not been found - presumably the excitation energy involved is too great for even metastability within this supercell.)

All of the other excited structures found in the calculations relate to variations in Jahn-Teller distortions and affect only the In-In and Zn-In bond lengths. They involve no significant changes in vacancy volume, Zn position or electron occupancy of the complex (see next subsection). The energies involved are very small indeed - on or below the order of room temperature thermal energies. Room temperature experiments are therefore likely to see averages over these structures. Three possible structures are found to be stable - one In-In bond dimerised (the other two equal), one antidimerised or all equal. How the symmetric structure comes to be stable despite the Jahn-Teller effect will be returned to in section V. All three structures are found to be stable for $Q = -1$ and $Q = -3$, but for $Q = -2$ the symmetric structure is not seen. For $Q = 0$ and +1 we find only the symmetric structure.

The energy separations between these structures are

TABLE V: Ab initio results for the Lowest Lying structures (marked L.L.) of $[\text{Zn}_{\text{In}}\text{-V}_{\text{P}}]^Q$ for $Q = +2 \rightarrow -4$, together with structural excitation energies in electron volts. DM = dimerised, SY = symmetric, AD = antidimerised. "-" indicates that the structure is not stable.

Q	DM	SY	AD
+2	-	L.L.	-
+1	-	L.L.	-
0	-	L.L.	-
-1	L.L.	0.0004	0.0001
-2	0.0002	-	L.L.
-3	0.0097	0.0104	L.L.
-4	-	L.L.	-

on the limits of what we expect to resolve using only the 2x2x2 Monkhorst-Pack k-point grid together with equation 5. As a result we have re-calculated the energies and structures of all of these states using a 4x4x4 k-point Monkhorst-Pack grid, and, for some, even a 6x6x6 grid. We find that all of the structures reported in table III and IV remain stable, although the degree of dimerisation or antidimerisation changes in some cases. The order of stability for the three structures changes for $Q = -1$ and $Q = -3$, however, and in all charge states they move closer to degeneracy. These changes are illustrated in table V.

B. Charge density differences.

In figure 3 we show the instantaneous change in charge density when an electron is added to (upper row) or removed from (lower row) the $Q = 0$ charge state. In other words, we first take the $Q = 0$ relaxed positions and calculate with the $Q = -1$ or $Q = +1$ total charge. We then subtract from this new charge density the original charge density from the relaxed $Q = 0$ calculation. The isocharge surfaces plotted are for 80%, 50% and 20% of the peak value. It is clear that an electron added goes to a localised orbital on or near the In triangle. An electron removed, however, comes from a delocalised state. We note, however, that even for the 20% peak value isocharge surface for 0/-1, the total charge enclosed corresponds to only 0.48 electrons. Hence, even for the $Q = -1$ charge state, most of the added electron has an apparently delocalised character. This is, however, a result of the use of a relatively small supercell: the In-In distance is 3.7 Å *within* the cell, but about 9.2 Å *between* cells. This produces a significant fake dispersion for the defect levels, and means that the transfer levels given in table II should not be trusted too heavily.

In figure 4 we show the 50% peak isocharge surface for the instantaneous charge density change upon adding or removing electrons from the symmetric structures for $Q = +1$, 0 and -1. The orbital filled when adding an electron to $Q = 0$ and that emptied when removing an electron from $Q = -1$ are essentially the same. Clearly

$Q = -1$ is a localised state of the $[\text{Zn}_{\text{In}}\text{-V}_{\text{P}}]$ complex. Adding an electron to the $Q = -1$ state gives a very similar shaped charge density - the opposite spin state of the same orbital.

Removing an electron from $Q = 0$ empties a delocalised valence band state, as can be anticipated from the transfer level being found inside the valence band in the previous section. However, adding an electron to the (fully relaxed) $Q = +1$ fills an In triangle localised orbital, none the less. Clearly $Q = +1$ also corresponds to a localised state of the complex.

Going beyond +1 and -1, figure 4 also indicates a pattern which we in fact find for all charge states from +6 to -6: the electrons added or removed at the transfer levels +2/+1 and +1/0 come from essentially the same orbital, which we shall call Φ_0 . The same is also true for the orbitals corresponding to the transfer level pairs 0/-1 and -1/-2, (Φ_1), -2/-3 and -3/-4 (Φ_2) and -4/-5 with -5/-6 (Φ_3). Rather than plot all of them we show only one example of each orbital (transfer level pair). For the first three of these orbitals the shape is best seen in a top view, looking down the (111) axis. This is shown in figure 5 for the symmetric, dimerised and antidimerised structures. A clear relationship emerges: the dimer orbital for 0/-1 is very similar to the antidimer orbital for -2/-3. Likewise, the dimer orbital for -2/-3 and the antidimer orbital for 0/-1 are the same. Furthermore, a symmetric combination (addition) of these two would give an orbital very much like that of the symmetric -2/-3 orbital. An antisymmetric combination (subtraction) would give something similar to the symmetric orbital for 0/-1, although in this case the similarity is not complete. This may be due to differences in the degrees of dimerisation or perhaps to limitations in the calculation. Despite this, a clear relationship between the orbitals filled/emptied at these transfer levels in the three nearly degenerate structures is present and will be considered in more detail in section V.

For the orbital associated with -4/-5 and -5/-6 we show a side view in figure 6. It is the Zn $2p^z$ orbital, as expected based upon the structures reported in the previous section. Confirming this now allows us to fully explain the volume dependence of the complex, as shown in table III. The volume is reduced monotonically from $Q = +2$ to $Q = -6$. For $Q = -4 \rightarrow -6$ this is due simply to the change from DX to non-DX - as the Zn $2p^z$ orbital fills up, the sp^2 bonding to the P atoms is reorganised, with a normal sp^3 dangling bond developing. This can then bond on a more or less equal footing with the In dangling bonds. Then from $Q = +2 \rightarrow -4$ the In-In distances are reduced as electrons enter the In dangling bonds, increasing the bonding between them. The volume reduction, however, is due only partly to this: partly it is due to the concurrent reduction in Zn-In distances, even though no bonds form between the Zn and In until $Q = -5$. This reduction is electrostatic in origin. The empty Zn $2p^z$ orbital, together with the relatively high ionicity of the Zn-P bonds, (see figure 2,) leaves the positive Zn core

slightly less well screened along the direction pointing towards the three In atoms. The negative charge on the In atoms, meanwhile, increases as electrons are added, so the Zn-In distance is reduced electrostatically. Thus the reduction in effective vacancy volume at the 0/-1 transfer level, believed to have been observed in the positron annihilation studies,² is due to a combination of the In-In bonding and Zn-In electrostatic attraction, rather than to a DX to non-DX transition.

Regarding the other structures in tables III and IV, we find that, as anticipated from the structures themselves, the orbitals filled by adding further electrons to $[\text{Zn}_{\text{In}}\text{-V}_{\text{P}}]^{-6}$ or removing further electrons from $[\text{Zn}_{\text{In}}\text{-V}_{\text{P}}]^{+2}$ are all delocalised. We show only one example in figure 6, namely removing an electron from +5. The orbital filled by removing an electron to the metastable shrunken structure of $Q = +2$ (also in figure 6) is identical to that associated with removing an electron from the ground structure of $Q = +0$. This confirms the explanation given above of these shrunken structures in terms of holes excited off into delocalised valence band states.

V. STRUCTURAL MODEL FOR THE $[\text{Zn}_{\text{In}}\text{-V}_{\text{P}}]$ COMPLEX.

A. Symmetry considerations.

Since, for $Q > -5$, the Zn is in a DX-like position and the Zn $2p^z$ is much higher in energy than the other orbitals involved, we omit it, and base our model on the assumption that all additional electrons added/removed from the complex go to/come from the triangle of sp^3 hybrid dangling bonds on the In atoms. These start out life transforming as the 0^+ (s) and 1^- (p) irreducible representations of the O_3 group for the free atoms, which descend to the (1 dimensional) A_1 and (3 dimensional) T_2 representations of the tetragonal group T_d when placed inside a zinc blend structured crystal. (See the level splitting diagram in figure 7.) The point group of a free vacancy (without the Zn) is the same - T_d - and so the bound states inside the vacancy are known to also be described¹⁷ by the same A_1 and T_2 representations of T_d - giving a deep symmetric level and a three-fold degenerate excited level. (Jahn-Teller distortions lifting this degeneracy lead to the negative U effects for the free V_{P} .) In $[\text{Zn}_{\text{In}}\text{-V}_{\text{P}}]$ the Zn further lowers the point group to C_{3v} . The A_1 representation of T_d is projected onto the A_1 representation of C_{3v} , whilst the T_2 representation splits, giving a second A_1 representation and a 2 dimensional E representation. The two A_1 representations can mix, so that the hybridisation on the Zn is reorganised, to give the high (unoccupied) Zn $2p^z$ orbital observed in our calculations, plus a new totally symmetric level constructed primarily from the three remaining In dangling bonds. The E representation corresponds to a two-fold

degenerate excited state, also constructed primarily from In dangling bonds. In the neutral state the lowest A_1 level is full and the others are empty. For charge states $Q = -1 \rightarrow -3$ this degeneracy must also be lifted, usually by a further structural Jahn-Teller effect. This can happen in two ways - via the formation of one stronger or one weaker bond, leading to the C_{1v} point group, or via a process reducing the symmetry to C_3 , splitting the E level into $l = \pm 1$ components. The latter requires a rigid rotation of the In triangle around the (111) axis, alternately shortening and lengthening the In-P bonds in the plane perpendicular to (111). This is not likely to be favoured, however, since the energy gained would be very small. Indeed, we do not see any tendency towards this in our ab initio structures.

For certain Q it is also possible for the degeneracies to be lifted by spin interactions. In the $Q = -1$ state, where the In triangle contains 3 electrons, it would be possible to localise one electron on each In - making the lower A_1 and E representations degenerate - and then form an $S = \frac{3}{2}$ high spin state. This would require¹⁸ the In sp^3 dangling bonds to be spatially rather small (localised) and hence local Coulomb interactions to be rather strong. This does not appear to be the case, however. In additional calculations using the Local Spin Density Approximation (LSDA) to search for it we find no evidence of such a state being stable. Similarly, in $Q = -2$, with 4 electrons present, an $S = 1$ high spin state could be formed in the half filled T_2 . Again, we find no indications that this is stable.

Instead, it seems that the symmetric structures for $Q = -1 \rightarrow -3$ are stabilised by weak Coulomb interactions with no localisation. We can estimate the differences between the classical spatial overlaps of the three orbitals. Specifically, we take the charge contained in the overlap regions of the isocharge surfaces for charge density differences, (as plotted in figures 3-6)) renormalised to a whole electron to allow comparisons, and evaluate what fraction of the charge overlaps classically. Using the 50% isocharge surfaces in figure 5, we find that the highest orbital (corresponding to transfer levels -2/-3 and -3/-4) has 1.58 times as much overlap with the lowest (transfer levels +2/+1 and +1/0) as the middle orbital (0/-1 and -1/-2) has with the lowest. (The overlap between the middle and the highest is about 29 times larger again.) Using the 20% isocharge surface, where more of the actual charge is accounted for, but where the spurious defect level dispersion is starting to wash out the effect, we find that the lowest orbital has 1.62 times as much overlap with the highest as it has with the middle one. These numbers indicate that in the symmetric geometries the E level is split into orbitals having less and more overlap with the deep A_1 level. These levels are thus split by Coulomb repulsion from the electrons filling the deep A_1 level.

B. A tight binding model.

The Jahn-Teller behaviour found in the ab initio studies can be explained using a simple tight binding model. To do this we need only to consider the leading order effects of changes in the In-In distances. We make no assumptions yet about the form of the degenerate associated orbitals ϕ_i and we consider only the “hopping” overlap matrix elements t_{ij} which move electrons between the orbitals on In_i and on In_j . The Hamiltonian is simply

$$\hat{H} = \sum_{i,j;\sigma} -t_{i,j} c_{j,\sigma}^\dagger c_{i,\sigma} \quad (7)$$

where $c_{i,\sigma}^\dagger$ ($c_{i,\sigma}$) creates(annihilates) a spin σ electron at i , the sums being over the three In atoms. We make the selection $t_{23} = t + \delta$ and $t_{12} = t - \frac{\delta}{2} = t_{13}$. Hence $\delta > 0$ corresponds to forming a single $\text{In}_2\text{-In}_3$ dimer (plus two antidimers) and $\delta < 0$ to a single $\text{In}_2\text{-In}_3$ antidimer (plus two dimers). (The $-\frac{\delta}{2}$ terms balancing the $+\delta$ allow direct comparisons between $\delta > 0$, $= 0$ and < 0 .) We omit Coulomb repulsion (we assume that $U \ll t$) and also the spin-spin interactions which would lead to high spin states. On the other hand, we will treat the symmetric structures as (potentially) metastable, thus implicitly assuming the presense of (at least a) vanishing Coulomb repulsion between the E levels and the deep A_1 level. More importantly, we also omit elastic effects from the lattice. To leading order, δ is linear in the change in In-In distance, but the elastic energy is quadratic. We can therefore write the elastic energy for an individual bond between In_i and In_j as $\lambda \delta_{ij}^2 t$, where λ is (related to) an elastic constant. Hence for both the dimer and antidimer states described above the elastic energy is $\approx \lambda \delta^2 t + 2\lambda \left(\frac{\delta}{2}\right)^2 t = \frac{3\lambda \delta^2 t}{2}$. However, we omit this term at present, solving only equation 7.

In the dimer case ($\delta > 0$) the solution is:

$$\begin{aligned} E_0 &= -\frac{1}{2} - \frac{\delta}{2} - \frac{F(\delta)}{2} \approx -2 - \frac{\delta^2}{6} \\ E_1 &= -\frac{1}{2} - \frac{\delta}{2} + \frac{F(\delta)}{2} \approx 1 - \delta + \frac{\delta^2}{6} \\ E_2 &= 1 + \delta \end{aligned} \quad (8)$$

in units of t , (expansions to $O(\delta^2)$ only) where

$$\begin{aligned} F(\delta) &= \sqrt{3}\sqrt{3 - 2\delta + \delta^2} \\ &\approx 3 - \delta + \frac{\delta^2}{3} \end{aligned} \quad (9)$$

We write the wavefunctions in the form $\Phi = (a_1, a_2, a_3)$ where $\{a_i\}$ are the coefficients of $\{\phi_i\}$ in Φ . The wavefunctions associated with E_0 , E_1 and E_2 are thus

$$\begin{aligned} \Phi_0 &= \left(\frac{1+\delta-F(\delta)}{\delta-2}, 1, 1 \right) \approx \left(1 - \frac{\delta}{2} - \frac{\delta^2}{12}, 1, 1 \right) \\ \Phi_1 &= \left(\frac{1+\delta+F(\delta)}{\delta-2}, 1, 1 \right) \approx \left(-2 - \delta - \frac{2\delta^2}{3}, 1, 1 \right) \\ \Phi_2 &= (0, 1, -1) \end{aligned} \quad (10)$$

respectively. (Normalisation is omitted for clarity.) Hence, the ground state E_0 is totally bonding, (an A_1 irreducible representation of C_{1v}), but has more weight upon the dimerised $\text{In}_2\text{-In}_3$ bond, thus corresponding to a dimer bonded to the single site In_1 . This is a very different result to that obtained^{6,7,15} for the free Vp , where the lowest lying state was totally symmetric with equal weight on all sites. This new result for $[\text{ZnIn-Vp}]$ indicates that a dimer (or antidimer) may form even with only one electron present and no degeneracy. (The Jahn-Teller theorem does *not* state that symmetry *cannot* be reduced in the absence of degeneracy.) This possible symmetry lowering is weak, however: the energy gained is only $\sim \delta^2$, the same order as the elastic energy lost. It comes about because the dimerisation/antidimerisation breaks the E irreducible representation of C_{3v} up into a B_1 and a further A_1 representation of C_{1v} . This new A_1 representation can mix with the other ones, leading to a weak gain in energy, even though Jahn-Teller does not actually require it here. Taking elastic energy into account, the total energy of the dimer structure for $Q = +1$ (with one electron) is

$$E^{Q=+1} = -\frac{t}{2} (1 + \delta + F(\delta) - 3\lambda\delta^2) \quad (11)$$

Taking the derivative of $E^{Q=+1}$ with respect to δ we find that the lowest energy solution has $\delta > 0$ (is dimerised) as long as $0 < \lambda < 0.17$. This appears to correspond to a weak value of the elastic constant. For $Q = -1 \rightarrow -3$ a stable dimer state exists for any value of λ and has a lower energy than the symmetric structure. Our DFT calculations indicate that the case of $[\text{ZnIn-Vp}]$ in InP is near to this critical value of $\lambda = 0.17$: if we do the relaxation using a $4 \times 4 \times 4$ k-point grid we do not find a stable dimer or a stable antidimer. However, if we use the less accurate $2 \times 2 \times 2$ k-point grid we do indeed find a non-symmetric structural groundstate for $Q = +1$, namely a 2.1% dimerised structure, with the symmetric structure an excitation 0.002 eV above. For $Q = +0$ we never find stable dimerised or antidimerised structures.

Turning to the model excitations for the dimer structure, E_1 also corresponds to an $\text{In}_2\text{-In}_3$ dimer, (another A_1 representation,) but now anti-bonded to the single site, upon which most of the weight is placed. E_2 is an antibonded dimer (an antidimer - a B_1 irreducible representation of C_{1v}) with no weight at all on the single site. For the antidimer structure ($\delta < 0$) the groundstate remains the same (at least for small δ) but there is less weight on the dimer bond and more on the single site. Also, the order of the excitations is reversed, with the antidimer state (E_3 above) becoming the lower of the two. If we now assume a form for ϕ_i related to sp^3 hybrids we can see what sort of charge densities we expect to see for the Φ_j , as sketched in figure 8.

In the case of the excitations for the symmetric structure, we find

$$\Phi_{1,2} = \Phi_{\pm} = \left(1, e^{\pm \frac{2\pi}{3}i}, e^{\pm \frac{4\pi}{3}i} \right) \quad (12)$$

with the two being, of course, degenerate. Unfortunately, describing the lifting of this degeneracy as a result of Coulomb and elastic effects (the two will almost certainly combine) lies well outside the scope of this model or paper. Hence what is shown in the figure is just the two alternatives with C_3 symmetry and three node-like planes, based upon the form of Φ_{\pm} . The one with low charge density along the In-In lines is likely to have a smaller overlap with - and hence Coulomb repulsion from - the symmetric E_0 groundstate. Hence it has been drawn as the lower of the two excitations. This cannot be predicted with more certainty upon the basis of the current model calculation, however.

With the obvious exception of the excitations for the symmetric structure, the similarity between the model charge densities in figure 8 and the ab initio charge densities in figure 5 is obvious. We are indeed seeing the predicted combinations of one electron orbitals from the three dangling In dangling bonds, controlled by Jahn-Teller effects which the model can also predict.

Using equation 9 we can now evaluate the energy of the symmetric, dimerised and antidimerised states for each value of electron filling and compare them. For example, with five electrons present ($[\text{Zn}_{\text{In}}\text{-V}_{\text{P}}]^{-3}$) the symmetric state has energy $-t$, the dimerised state has energy $-t(1 + \delta)$ and the antidimerised state has energy $-\frac{t}{2}(1 + \delta + F(\delta)) \approx (-t(1 + \delta + \frac{\delta^2}{6}))$. Hence the lowest is the antidimer, with the dimer as an excitation only $\sim \frac{\delta^2 t}{6}$ higher, and the symmetric state lies $\sim \delta t$ higher still. Comparing to table V we indeed see that the antidimer is the most stable, followed by the dimer, with the symmetric structure the least stable. Table VI shows the leading terms in these excitation energies for fillings of 0 to 6 electrons. Since both elastic and Coulomb energies favour the symmetric structure we anticipate only the symmetric structure for $Q = +2$ and -4 , as observed. We also anticipate that the excitation energies for the symmetric forms will be lower than those indicated in the table. We find that for 1 or 2 electrons the dimerised structure to be the most stable, closely followed by the antidimerised structure. For 3, 4 or 5 electrons we expect the antidimerised structure to be the lowest, with the symmetric structure always the least. The agreement with the ab initio results is very close - the only real exception is that for $Q = -3$ our ab initio calculations found the dimerised state to be slightly more stable than the antidimerised. The ab initio energy difference was tiny, however, over an order of magnitude less than the accuracy anticipated from such a calculation. On the other hand, the model does predict that the symmetric structure is at its least stable for charge $Q = -2$ and this is indeed the only charge state for which we are unable to find the symmetric structure using DFT.

TABLE VI: Model predictions for the lowest lying structures (marked L.L.) of $[\text{Zn}_{\text{In}}\text{-V}_{\text{P}}]^Q$, together with structural excitation energies to leading order in δ , for occupancies of 0 to 6 electrons ($\# e^-$). DM = dimerised, SY = symmetric, AD = antidimerised.

$\# e^-$	Q	DM	SY	AD
0	+2	-	L.L.	-
1	+1	L.L.	$\frac{\delta^2 t}{6}$	$\frac{\delta^3 t}{9}$
2	0	L.L.	$\frac{\delta^2 t}{3}$	$\frac{2\delta^3 t}{9}$
3	-1	$\frac{\delta^2 t}{6}$	δt	L.L.
4	-2	$\frac{\delta^2 t}{3}$	$2\delta t$	L.L.
5	-3	$\frac{\delta^3 t}{6}$	δt	L.L.
6	-4	-	L.L.	-

VI. CONCLUSIONS.

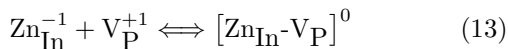
We have calculated the structure and transfer levels of the $[\text{Zn}_{\text{In}}\text{-V}_{\text{P}}]$ complex using ab initio DFT methods and have presented detailed results for the dependence of the structure and structural excitations upon the charge state of the complex and hence upon the Fermi level. We found that, for all charge states below -5, the Zn atom lies in a DX position, sp^2 hybridised, with an empty $2p^z$ orbital directed towards the In triangle and very constant bond lengths to the surrounding P atoms. Electrons added (below $Q = -5$) go into localised orbitals built from the three In dangling bonds - thus reducing the In-In distances with each added electron. We also found that there is a simultaneous reduction in the Zn-In distances, which is of electrostatic in origin. This was due to the increased charge on the In triangle and the weaker screening of the Zn core along (111) owing to the empty Zn $2p^z$ orbital. The combination of these effects leads to a systematic reduction in the effective vacancy volume of the complex for charge states from $Q = +2 \rightarrow -4$. This is in spite of the fact that the DX structure of the complex remains stable with rising Fermi level right up until a -4/-6 negative U transfer level, about 0.5 eV into the conduction band. For charge states $Q = -1 \rightarrow -3$ we also found complex Jahn-Teller behaviour, with up to three different stable structures - symmetric, dimerised and antidimerised - which are all very close to degeneracy. For $Q = -1$ the most stable structure (just) is dimerised, whilst it is antidimerised for $Q = -2$ and -3.

In addition, we have presented a simple tight binding model which is able to predict and explain all of the structural properties of the complex - including the existence of three possible nearly degenerate structures for $Q = -1 \rightarrow -3$. Such a near degeneracy between dimer and antidimer structures has not been seen for the free V_{P} and this too the model can predict: the same model applied to V_{P}^{-1} , for example, shows a separation between dimerised and antidimerised structures on the order of δ , compared to δ^2 here for $[\text{Zn}_{\text{In}}\text{-V}_{\text{P}}]$. (Details of these calculations will be presented elsewhere.¹⁵) Success with such a simple model is very pleasing and may in the fu-

ture even help to narrow the range of initial configurations required when searching for structural minima in similar ab initio calculations.

Comparing our results to those obtained experimentally using positron annihilation, we, as they, find that the most stable charge state of the $[\text{Zn}_{\text{In}}\text{-V}_{\text{P}}]$ complex is $Q = 0$ in p-type material. We find a binding energy of 0.39 eV which is also in the range they anticipate. Regarding the structure of the complex, we, as they, find a larger effective vacancy volume than that of the free V_{P} . Upon excitation to the -1 charge state we, as they, see a reduction in volume. At 0.50 eV our 0/-1 transfer level is a little high for agreement, but, as was noted, these transfer levels are not reliable since the supercell is too small. Further studies of the complex in larger cells are required to check how this effects the position of the transfer levels, but our results seem otherwise to be in very good agreement with the experiments.

Regarding the issue of compensation, our results confirm that, should free V_{P} somehow be present in heavily Zn-doped InP, they would indeed form stable complexes with Zn. However, the formation energy we find for V_{P} is 1.96 eV, which is still rather large. Even for a phosphorus atom neighbouring a Zn dopant the effective formation energy is $1.96 - 0.39 = 1.57$ eV, which is not small. The positron annihilation experiments clearly demonstrate that at least some V_{P} are present in heavily Zn doped Czochralski grown InP. However, the lack of a low formation energy leaves it unclear whether, and perhaps unlikely that, V_{P} generation is the primary cause of compensation in InP:Zn. On the other hand, our DFT results indicate that the formation of $[\text{Zn}_{\text{In}}\text{-V}_{\text{P}}]$ complexes from existing Zn_{In} and V_{P} is certainly *not* responsible for compensation: starting with fully ionised Zn, the complex forming reaction is



in which no free electrons or holes are created or absorbed. The compensation issue here has to do with the formation of the phosphorus vacancies in the first place, and is not affected by the formation of the $[\text{Zn}_{\text{In}}\text{-V}_{\text{P}}]$ complex. Fully understanding the issue of carrier compensation in InP:Zn from an ab initio point of view may thus require more work.

VII. FIGURE CAPTIONS.

A. Figure 1.

Structure of the supercell containing the neutral $[\text{Zn}_{\text{In}}\text{-V}_{\text{P}}]$ complex. Atom types are dark grey: In, pale grey: P, black: Zn.

B. Figure 2.

ELF plots for the neutral $[\text{Zn}_{\text{In}}\text{-V}_{\text{P}}]$ complex. For clarity most atoms are omitted and the edges of the Zn-In tetrahedron are drawn. Note, however, that there are *no* Zn-In bonds. a) ELF in a plane containing Zn, 1 In and the (111) axis. b) ELF in a plane containing Zn and 2 In.

C. Figure 3.

Charge density difference plots for the $[\text{Zn}_{\text{In}}\text{-V}_{\text{P}}]$ complex in the $Q = 0$ relaxed geometry, but with an extra electron added (upper row) or removed (lower row). Shown are isocharge surfaces for the charge density difference itself. The surfaces shown are for 80%, 50% and 20% of the peak value.

D. Figure 4.

50% isosurface plots for charge density differences for adding (top row) and removing (bottom row) electrons from the $Q = +1, 0$ and -1 relaxed structures for $[\text{Zn}_{\text{In}}\text{-V}_{\text{P}}]$.

E. Figure 5.

Top views (down the (111) axis) of the 50% isosurface plots for charge density differences corresponding to the transfer levels of $[\text{Zn}_{\text{In}}\text{-V}_{\text{P}}]$ from $Q = +2$ to -4 , for the symmetric, dimerised and antidimerised structures.

F. Figure 6.

Side views of charge density difference plots for a) the Zn $2p^z$ related orbital filled at the $-4/-5$ and $-5/-6$ transfer levels, b) the delocalised orbital emptied in removing an electron from $Q = +5$ and c) the orbital emptied in removing an electron from the metastable shrunken structure for $Q = +2$.

G. Figure 7.

Irreducible representation splittings as symmetry is lifted from O_3 to C_{1v} or C_3 . For C_{1v} the dimer case is shown. For the antidimer the B_1 level lies below the second A_1 level.

H. Figure 8.

Sketch of the wavefunctions anticipated for the three structures of $[\text{Zn}_{\text{In}}\text{-V}_{\text{P}}]$, based upon the model. (DM =

FIG. 1:

dimerised, SY = symmetric, AD = antidimerised.)

FIG. 2:

-
- * Current address Material Physics, Kungliga Techniska Hgskolan, 229 KTH-Electrum, 16440 Kista.; Electronic address: Christopher.Castleton@fysik.uu.se
- ¹ J. Mahony, P. Mascher, and W. Puff, *J. Appl. Phys.* **80**, 2712 (1996).
 - ² J. Slotte, K. Saarinen, A. Salmi, S. Simula, R. Aavikko, and P. Hautajarvi, Preprint, to appear in *Phys. Rev. B* (2003).
 - ³ K. Saarinen, Private Communications. (2001).
 - ⁴ M. Alatalo, H. Kauppinen, K. Saarinen, M. Puska, J. Mkinen, P. Hautajarvi, and R. Nieminen, *Phys Rev B* **51**, 4176 (1995).
 - ⁵ R. Jansen, *Phys. Rev. B* **41**, 7666 (1990).
 - ⁶ M. Alatalo, R. Nieminen, M. Puska, A.P. Seitsonen, and R. Virkkunen, *Phys. Rev. B* **47**, 6381 (1993).
 - ⁷ A.P. Seitsonen, R. Virkkunen, M. Puska, and R. Nieminen, *Phys. Rev. B* **49**, 5253 (1994).
 - ⁸ W. Kohn and L. Sham, *Phys. Rev.* **140**, A1133 (1965).
 - ⁹ D. Vanderbilt, *Phys. Rev. B* **41**, 7892 (1990).
 - ¹⁰ G. Kresse and J. Hafner, *J. Phys.: Cond. Matt.* **6**, 8245 (1994).
 - ¹¹ G. Kresse and J. Furthmuller, *Comp. Mat. Sci.* **6**, 15 (1996).
 - ¹² Adapted, from S.B. Zhang, and J. Northrup, *Phys. Rev. Lett.* **67**, 2339 (1991).
 - ¹³ H. Monkhorst and J. Pack, *Phys. Rev. B* **13**, 5188 (1976).
 - ¹⁴ B. Silvi and A. Savin, *Nature* **371**, 683 (1994).
 - ¹⁵ C. Castleton and S. Mirbt, In preparation. (2003).
 - ¹⁶ C. Castleton, Unpublished. (2001).
 - ¹⁷ M. Lannoo, *Physica B* **116**, 63 (1982).
 - ¹⁸ A. Zywietz, J. Furthmuller, and F. Bechstedt, *Phys. Rev. B* **59**, 15166 (1999).
 - ¹⁹ Alatalo et al. have^{2,4} used DFT-LDA and DFT-GGA calculations to estimate the positron annihilation at Zn-V_P complexes, but they included only empiracle breathing mode relaxations (to fit the positron lifetimes) and presented no results for the structure, transfer levels or energetics of the complex.
 - ²⁰ Bulk values are calculated using the same pseudopotentials as we use for the defect calculations, but they are each fully converged in terms of both k-point grid and planewave cutoff.
 - ²¹ Certain additional structures - a dimerised structure for $[\text{Zn}_{\text{In}}\text{-V}_P]^{+1}$, dimerised and antidimerised structures for $[\text{Zn}_{\text{In}}\text{-V}_P]^{-4}$ and a second weaker dimer structure for $[\text{Zn}_{\text{In}}\text{-V}_P]^{-2}$ - are found when the 2x2x2 Monkhorst-Pack k point grid is used. However, these turn out to be unstable when recalculated using a 4x4x4 k point grid.

FIG. 3:

FIG. 4:

FIG. 5:

FIG. 6:

FIG. 7:

FIG. 8:

This figure "figure1.jpg" is available in "jpg" format from:

<http://arxiv.org/ps/cond-mat/0303038v1>

This figure "figure2.jpg" is available in "jpg" format from:

<http://arxiv.org/ps/cond-mat/0303038v1>

This figure "figure3.jpg" is available in "jpg" format from:

<http://arxiv.org/ps/cond-mat/0303038v1>

This figure "figure4.jpg" is available in "jpg" format from:

<http://arxiv.org/ps/cond-mat/0303038v1>

This figure "figure5.jpg" is available in "jpg" format from:

<http://arxiv.org/ps/cond-mat/0303038v1>

This figure "figure6.jpg" is available in "jpg" format from:

<http://arxiv.org/ps/cond-mat/0303038v1>

This figure "figure7.jpg" is available in "jpg" format from:

<http://arxiv.org/ps/cond-mat/0303038v1>

This figure "figure8.jpg" is available in "jpg" format from:

<http://arxiv.org/ps/cond-mat/0303038v1>